LRP 446/91 APRIL 1992

IDEAL MHD STABILITY OF INTERNAL KINKS IN CIRCULAR AND SHAPED TOKAMAKS

H. Lütjens, A. Bondeson and G. Vlad

submitted for publication in

NUCLEAR FUSION

IDEAL MHD STABILITY OF INTERNAL KINKS IN CIRCULAR AND SHAPED TOKAMAKS

H. Lütjens, A. Bondeson

Centre de Recherches en Physique des Plasmas,
Association Euratom - Confédération Suisse, Ecole Polytechnique Fédérale de Lausanne,
21 Av. des Bains, CH-1007 Lausanne, Switzerland

G. Vlad

Associazione Euratom - ENEA sulla Fusione, C.R.E. Frascati,
C.P. 65-00044 - Frascati, Rome, Italy

Abstract: Stability limits for the internal kink mode in tokamaks are calculated for different current profiles and plasma cross sections using ideal magnetohydrodynamics (MHD). The maximum stable poloidal beta at the q = 1 surface (β_p) is sensitive to the current profile, but for circular cross sections, it is typically between 0.1 and 0.2. Large aspect ratio theory gives similar predictions when the appropriate boundary conditions are applied at the plasma-vacuum surface. The pressure driven internal kink is significantly destabilized by ellipticity. For JET geometry, the β_p-limit is typically between 0.05 and 0.1, but arbitrarily low limits can result if the shear is reduced at the q = 1 surface. A large aspect ratio expansion of the Mercier criterion retaining the effects of ellipticity and triangularity is given to illustrate the destabilizing influence of ellipticity.

1. INTRODUCTION

Ideal MHD theory has been successful in predicting the global pressure limit for tokamaks. However, for the stability of the central region, where the n = 1 internal kink mode can become unstable and trigger the so-called sawtooth oscillations, the theoretical understanding is at present very incomplete. The uncertainties are manyfold: no clear understanding of what is the appropriate physics model; poor knowledge of the current profile, to which the internal kink is highly sensitive; and incomplete knowledge of the stability limits even in the simplest theoretical model - ideal MHD. In this paper, we present a numerical and analytical study with the aim of clarifying the stability properties of the internal kink within the ideal MHD model. Our main result is that the pressure limit is lower than previously thought.

Bussac et al [1] calculated the pressure limit for internal kink stability by a large aspect ratio expansion. For a circular cross section, parabolic current profile and a small q = 1 radius, they found that the mode is stable when $\beta_p < (13/144)^{1/2} \approx 0.3$. For other current profiles, the large aspect ratio expansion predicts limits between 0 and 0.1 [2,3]. In this paper, we reconsider the large aspect ratio calculation for the same profiles as in Ref. [1]. Our results differ from those of [1] because of a difference in boundary conditions. We assume the q = 2 surface always lies within the conducting plasma. Thus, when q(a) < 2, we replace the conducting wall at r = a in [1], by a perfectly conducting, currentless plasma that extends beyond the q = 2 surface. With this prescription, rounded current profiles give a β_p-limit that is typically between 0.1 and 0.2. This limit decreases monotonically with increasing q = 1 radius and for q_0 below some profile-dependent threshold, the n = 1 internal kink is unstable at zero beta [4].

With respect to shaping, analytical studies [3, 5] suggest that the effect of ellipticity is weak when the central safety factor q_0 is close to unity, whereas numerical computations indicate a strong effect [6 - 8]. Our numerical calculations, without recourse to geometrical orderings, confirm that ellipticity is strongly destabilizing, in particular, at low shear. The destabilization appears to be connected to interchange effects which are disregarded in the standard large aspect ratio expansion. We give a modified large aspect ratio expression for the Mercier criterion which includes the effects of ellipticity and triangularity.

2. CIRCULAR CROSS SECTION - CURRENT PROFILE EFFECTS

2.1 Large aspect ratio expansion

For circular equilibria, stability limits for the internal kink mode have been calculated by means of the large aspect ratio expansion [1], however, rather different limits in β_p were found for different current profiles [1-3]. For a parabolic current profile, Bussac et al [1] found a limit of about 0.3 when $r_{q=1} \ll a$ which falls to a minimum of 0.23 for $r_{q=1}/a \approx 0.4$ and then increases again for larger q = 1 radii. For profiles that are more peaked than parabolic, the pressure limit decreases more sharply with $r_{q=1}$. Very steep current profiles, such as the Shafranov (step-function) profile are more unstable. The β_p-limit for the Shafranov profile has a maximum of about 0.095 for $q_0 \approx 0.9$, and falls to zero at an upper and lower limit in q_0: 1 and about 0.58 [3].

The stability diagram ($\beta_{p,crit}$ vs. $r_{q=1}/a$) of Bussac et al [1] was computed assuming a fixed plasma boundary. Thus, the m = 2 perturbation induced by toroidal coupling is wall stabilized whenever $q_a < 2$ (q_a is the safety factor on the plasma surface, r = a). For the parabolic current profile, $q_a/q_0 = 2$, and therefore $q_a < 2$ occurs whenever $q_0 < 1$ (i.e., when the internal kink is of interest). Thus, the results for the parabolic profile in [1] refer to non-standard case of very-low-q operation, $q_a < 2$ with a close-fitting wall. Although tokamaks can be operated this way, the standard operating regime is $q_a > 2$. All calculations presented in this paper assume $q_a > 2$.

For comparison with the numerical results at finite aspect ratio, we have recomputed the large aspect ratio limit, using the boundary conditions appropriate for $q_a > 2$. Figure 1 shows the results for different current profiles: two polynomial profiles,

$$j(r) = \begin{cases} j_0(1 - r^2/a^2)^{\ell} , & r < a \\ 0 , & r > a \end{cases} \qquad (1)$$

with $\ell = 1, 2$ (parabolic and parabolic-squared), and the Shafranov profile, with the step placed at $r = r_0 = 0.5$ a. We assume that the q = 2 surface is always inside the conducting plasma. Thus, if $q_a < 2$ [$q_0 < 2/(\ell + 1)$ for the profiles (1)], we add a region of currentless but perfectly conducting plasma that extends to the q = 2 surface at $r/a = (2/q_a)^{1/2}$. (In this case, "a" denotes the radius of the current channel, not the plasma radius.) For the two smooth profiles (1), the β_p-limit falls monotonically when the q = 1

radius increases as shown in Fig. 1a. This is in contrast with the result if Ref. [1] for the parabolic profile, where the stabilization by the wall at r = a becomes stronger with increasing q = 1 radius, and the pressure limit even goes to infinity for $r_{q=1}/a > 0.79$. With the modified treatment of the wall, we find "typical" limits in the range of 0.1 to 0.2 rather than the usually quoted result 0.3 which is valid as $r_{q=1}/a \rightarrow 0$.

Figure 1 shows that the β_p-limit goes to zero for q_0 below some profile-dependent threshold, ranging from 0.40 for the parabolic-squared profile to 0.58 for the Shafranov profile. For q_0 close to unity, the pressure limit is highly sensitive to the current profile: the Shafranov profile gives a much lower value than the rounded-off current profiles (1).

2.2 Finite aspect ratio calculations - definitions

We have numerically calculated the full-MHD stability limits for the internal kink at finite aspect ratio using the stability code MARS [8] and the equilibrium code CHEASE [9]. The plasma vacuum surface in equilibrium is prescribed as

$$R = R_0 + a\cos(\theta + \delta \sin\theta) \quad , \qquad Z = a\,\kappa \sin\theta \quad , \tag{2}$$

where a is the minor radius, R_0 the major radius of the geometrical center, κ the elongation and δ the triangularity. In this paper, we present results for two geometries corresponding to he TEXTOR tokamak: $R_0/a = 4$, $\kappa = 1$, $\delta = 0$ (medium aspect ratio circle), and JET: $R_0/a = 2.7$, $\kappa = 1.7$, $\delta = 0.3$ (small aspect ratio dee).

In all cases, we have used the same pressure profile p/p_0. The pressure is prescribed as a function of the poloidal flux ψ, such that $dp/d\psi$ is constant in the central region and falls to zero smoothly at the edge. Figure 2 shows the pressure vs. the normalized minor radius $\rho \equiv [V(\psi)/V_{tot}]^{1/2}$, where $V(\psi)$ is the volume enclosed by a constant-ψ surface.

The current profiles are specified by the surface averaged toroidal current density,

$$I^* \equiv \frac{\int j_\phi\,(J/R)\,d\chi}{\int (J/R)\,d\chi} \quad , \tag{3}$$

[where J is the Jacobian for the transformation from flux coordinates (ψ, χ, ϕ) to Cartesian coordinates] as a function of the normalized poloidal flux ψ/ψ_{axis}. $I^*(\psi/\psi_{axis})$ is prescribed except for a multiplicative factor that is adjusted to specify the q = 1 radius.

Two important quantities for characterizing the equilibria are the shear

$$s \equiv \frac{\rho}{q}\frac{dq}{d\rho} \tag{4}$$

and the poloidal beta

$$\beta_p(\psi) \equiv -\frac{4}{\mu_0 I_\phi^2(\psi) R_m}\int_0^\psi \frac{dp}{d\psi'} V(\psi')\, d\psi' \ . \tag{5}$$

In (5), $I_\phi(\psi)$ is the toroidal current within a constant-ψ surface and R_m is the major radius of the magnetic axis. The poloidal beta at the q = 1 surface is denoted β_p.

The stability diagrams presented in the following give β_p as a function of the q = 1 radius $\rho_{q=1}$ at constant growth rates, $\gamma/\omega_A = 0$, 1×10^{-3}, 3×10^{-3} and 5×10^{-3}, where $\omega_A = v_A/R_0$ is the toroidal Alfvén frequency. These curves have been obtained after interpolation of $\gamma(\beta_p, \rho_{q=1})$ for equilibria with different values of β_p and identical I* profiles.

The results presented here have been obtained after convergence studies and extrapolation to zero mesh size, however, it should be noted that ideal-MHD growth rates of the order $10^{-3}\ \omega_A$ are non-trivial to compute. Our results for $\gamma = 10^{-3}\ \omega_A$ should be reliable, but in certain cases, extrapolation to marginal stability is somewhat uncertain. This may be acceptable from a physics point of view, since instabilities with very small growth rates must be expected to be strongly modified by non-MHD effects.

2.3 Numerical results for circular boundary

We have studied four different current profiles for plasmas with a circular boundary and a fixed aspect ratio of 4: one *rounded* profile, two profiles with I* *flattened* at a certain radius, and a *TEXTOR* profile where I* has "shoulders".

Figure 3 shows $I^*(\rho)$, $q(\rho)$ and $s(\rho)$ for the *rounded* profile, and the corresponding stability results are shown in Fig. 4. Both the current profile and the marginal stability curve are close to those for the parabolic-squared profile discussed in Sec. 2.1. Figure 4b shows the marginal β_p vs. q_0, to be compared with Fig. 1b.

Evidently, for an aspect ratio of 4 and circular boundary, the large aspect ratio theory is in good agreement with the full-MHD result.

Figure 5 shows the influence of the wall position for circular equilibria with $2 < q_a < 3$. The different curves show the growth rates of the n = 1 internal kink for different aspect ratios and a circular boundary, with the boundary either fixed or free (and the wall at infinity). For circular equilibria with $q_a > 2$, the large aspect ratio expansion shows no effect to lowest order of the wall position, and according to Fig. 5, this is a good approximation at large aspect ratio, A = 10. A detailed analysis of the numerical results shows that the difference in marginal β_p between the free and fixed boundary cases is proportional to $(a/R_0)^2$ at large aspect ratio. At tight aspect ratio, A = 2.7, the difference between the fixed and free boundary results is appreciable: $\beta_p \approx 0.1$ for free boundary and $\beta_p \approx 0.2$ for fixed boundary. The numerical results show a very weak influence of the wall position for circular equilibria with $q_a > 3$. In the following, we shall consider configurations where the wall is placed 20 % of the minor radius away from the plasma.

The two *flattened* current profiles have a plateau at a certain radius: $dI^*/d\rho = 0$ for $\rho \approx 0.42$. Inside this radius, the shear $s(\rho)$ is rather uniform, and on the outside, it increases sharply. We consider two profiles with different central shear: one with small central shear, $q_0/q(\rho=0.42) \approx 0.95$, and one with medium central shear, $q_0/q(\rho=0.42) \approx 0.80$.

Figure 6 shows $I^*(\rho)$, $q(\rho)$ and $s(\rho)$ for the flattened profile with low central shear at aspect ratio 4 and the stability results are shown in Fig. 7. The marginal values of β_p are similar to those for the rounded profile (Fig. 4) when the q = 1 surface is far away from the current plateau at $\rho \approx 0.42$, but when the q = 1 surface is near the plateau, the marginal β_p has a local minimum of about 0.08.

Figure 8 shows the stability for the flattened current profile with medium central shear. The equilibrium is similar to that in Fig. 6 except the central shear is four times larger. The limits in β_p are higher than for the low-shear equilibrium. They are quite similar to those for the rounded profile (Figs. 3 - 4), except for slightly higher values when the q = 1 radius is small, due to the higher shear near the magnetic axis.

Finally, Figs. 9 and 10 give profiles and stability results for a current profile of the *TEXTOR* type with shoulders at $\rho \approx 0.4$. The marginal β_p has a rather high maximum (≈ 0.46) when the q = 1 surface is located inside the shoulders, but the limit falls abruptly to values between 0.1 and 0.2 when the q = 1 radius increases and reaches the low-shear region. The TEXTOR profile is particularly stable to the internal kink mode and can even be resistively stable at fairly high β_p [8,10,11].

The large aspect ratio results in Sec. 2.1 show that the n = 1 mode is unstable even at zero pressure when q_0 is below a threshold value ranging from 0.58 for the Shafranov profile to 0.40 for the parabolic-squared profile. We have studied this purely current driven mode for two finite aspect ratio equilibria with zero pressure: (a) the rounded profile surrounded by a region of currentless but conducting plasma and (b) the Shafranov profile. The aspect ratios of the current channels (R_0/a and R_0/r_0, respectively) are 4 in both cases. Figure 11 shows the resulting growth rates as functions of q_0. Instability occurs below certain thresholds in q_0, which are in good agreement with the large aspect ratio result in Fig. 1. The instability at low q_0 has been observed previously by Turnbull and Troyon [4]. It is sensitive to the current profile, and the Shafranov profile is more unstable than the rounded profiles.

The results for circular equilibria can be simply summarized. Except at very low aspect ratio, the stability of the internal kink is in good agreement with the large aspect ratio theory. The β_p-limit decreases monotonically with increasing q = 1 radius (except in cases with non-monotonic or centrally very flat q-profile). With the appropriate treatment of the wall, typical β_p-limits lie between 0.1 and 0.2. The position of the wall makes a substantial difference only for tight aspect ratio and $q_a < 3$.

3. SHAPING EFFECTS

3.1 Numerical results for JET geometry

It is well known that internal kinks are destabilized by ellipticity [12]. To illustrate this, we give numerical results for the full ideal-MHD stability problem in JET geometry: aspect ratio A = 2.7, elongation $\kappa = 1.7$, and triangularity $\delta = 0.3$. We apply the same current profiles as for the circular cross section. The $q(\rho)$ and $s(\rho)$ profiles are slightly different from their circular equivalents, but the differences are insignificant in the central region, say $\rho < 0.6$.

The β_p-limits for JET geometry are generally significantly lower than for the circle. The results for the rounded current profile are shown in Fig. 12. The maximum stable β_p is about 0.09 and the limit decreases as the q = 1 surface approaches the magnetic axis. The effect of ellipticity was estimated analytically in Refs [3, 5] by computing the shaping contribution to δW at infinite aspect ratio and zero pressure. This shaping term was found to have a vanishing effect on the marginal β_p as $q_0 \rightarrow 1$. By contrast, the full-MHD result in Fig. 12 shows that the β_p-limit is strongly reduced for

JET shape and small q = 1 radius. In fact, with JET shape, $\beta_{p,crit}$ vanishes, or is very small, as q_0 approaches unity.

Similarly, for the two flattened current profiles, the beta-limits are lower with the JET cross section than for a circle, see Figs 13 and 14. The decrease is rather dramatic for the profile with weak central shear for which the β_p-limit in JET geometry is typically around 0.03, while the medium-shear profile gives about 0.08. Thus, contrary to expectation from the analytical expansions [3, 5], the destabilization is stronger in the case of weak central shear. This destabilization by shaping appears to be connected with interchange instability. The shaded region of Fig. 13 indicates violation of the Mercier criterion on the q = 1 surface. The minimum in $\beta_{p,crit}$ is clearly set by interchange instability for this equilibrium. It is well known [13] that, when the Mercier criterion is violated on a rational surface q = m/n, there exist unstable modes with toroidal mode number n. Our numerical calculations show that violation of the Mercier criterion on the q = 1 surface leads to an n = 1 internal kink, typically with a large growth rate.

Further evidence of the importance of interchange stability can be found in the stability diagram for the TEXTOR current profile, Fig. 15. This figure shows a dependence on shear locally at the q = 1 surface. The β_p-limit drops from about 0.17 (the highest value we have found with JET geometry) when the q = 1 surface is in the high-shear region inside the shoulders to about 0.03 when it enters the region of minimum shear. The minimum of the β_p-limit again coincides with the threshold for interchange at the q = 1 surface. The minimum in $\beta_{p,crit}$ increases if the minimum shear is increased, e.g., by reducing the shoulders in the current profile. Figure 16 shows the stability diagram for a TEXTOR profile with reduced shoulders and larger minimum shear ($s_{min} = s\ (\rho \approx 0.38) \approx 0.16$). Note the absence of a local minimum in the marginal β_p at the radius of minimum shear for this equilibrium.

We conclude that the ideal MHD pressure limit for the internal kink is significantly lower in JET geometry than for a circle. For most of the JET cases we have examined, the critical β_p is below 0.1. With elliptic shaping and weak shear, the Mercier criterion can be violated at low β_p, and this generally gives rise to global instabilities with large growth rates.

3.2 Large aspect ratio Mercier criterion including shape effects

Comparison of the numerical results for circular and JET-shaped cross section shows that ellipticity is destabilizing. The destabilization is particularly noticable at low shear, which appears to contradict the large aspect ratio results in [3, 5]. However, the shape corrections in [3, 5] were evaluated at infinite aspect ratio and zero pressure, while the destabilization of the internal kink in our numerical examples with low shear is connected with violation of the Mercier criterion on q = 1. This instability is well known: for vertically elongated flux surfaces, the Mercier criterion on the magnetic axis [14] is violated when q = 1, unless the triangularity is sufficiently large. It is evident that terms which are normally "small" in the large aspect ratio expansion can become non-negligible for equilibria with weak shear.

It would be desirable to express the ellipticity corrections to the potential energy of the internal kink by extending the large aspect ratio calculation of Bussac et al [1]. This entails retaining the toroidicity- and ellipticity-induced couplings of the m = 1 component to its four side-bands, m = -1, 0, 2, 3, and calculating all $O(\varepsilon^2 e)$ terms (where $\varepsilon = r_{q=1}/R_0$ and e is the ellipticity) in $\delta W/\varepsilon^2$. This is a rather formidable calculation, and, to illustrate the point, we shall content ourselves by giving the corrections to the Mercier criterion due to ellipticity and triangularity at large aspect ratio.

We modify the standard large aspect ratio expansion by introducing two small parameters: toroidicity, ε [$= r/R_0$], and ellipticity, e [$= (\kappa-1)/2$]. The poloidal beta and safety factor q will be considered as order one. The expansion will be taken to second order in ε and to first order in e, *keeping* the contributions of order $\varepsilon^2 e$. This is justified because the normally leading $O(\varepsilon^2)$ pressure contribution to the Mercier parameter vanishes for q = 1, so that the $O(\varepsilon^2 e)$ shaping terms give the leading contribution. We stress the importance of ordering ellipticity independently from aspect ratio. Connor and Hastie [5] set $e = O(\varepsilon)$ (so that, in the limit of infinite aspect ratio, the equilibrium is circular), and this makes the ellipticity-induced terms higher order in ε. The modified ordering allows us to calculate the ellipticity contribution without going beyond second order in ε.

Except for the difference in ordering, our calculation follows that of Connor and Hastie [5]. The flux surfaces are assumed to have the shape

$$R = R_0 - \varepsilon\,[r - e\,E(r)]\cos\omega - \Delta(r) + \varepsilon^2\,T(r)\cos 2\omega + \varepsilon^3\,P\cos\omega + \ldots\,,$$
$$Z = \quad \varepsilon\,[r + e\,E(r)]\sin\omega \quad + \varepsilon^2\,T(r)\sin 2\omega - \varepsilon^3\,P\sin\omega + \ldots\,, \tag{6}$$

where r and ω are two non-orthogonal coordinates corresponding to minor radius and poloidal angle, and ε and e are independent expansion parameters. The elliptic deformation E(r) is related to the elongation by $\kappa = 1 + 2E/r + O((E/r)^2)$, $\Delta(r)$ is the Shafranov shift, and T(r) is the triangular deformation related to the triangularity by $\delta = 4T(r)/r$. Keeping the terms up to second order in ε and first order in e, we obtain the Mercier criterion as $-D_I > 0$, where

$$-D_I = \frac{1}{4} + \frac{2p'}{rB^2}\frac{q^2}{q'^2}\left[1 - q^2 + \frac{3q^2}{4}\left(\frac{E}{r} + E'\right) + \frac{3q^2}{2}\Lambda\left(\frac{E}{r} - E'\right)\right.$$
$$\left. - \frac{R_0 q^2}{r}\left(\frac{2ET}{r^2} + \frac{6E'T}{r} + \frac{7ET'}{2r} - \frac{3}{2}E'T'\right)\right], \tag{7}$$

Details of the calculation are given in the Appendix. In (7), prime denotes differentiation with respect to the minor radius r and $\Lambda \equiv R_0\,\Delta'/r \approx \beta_p(r) + \ell_i(r)/2$, where $\ell_i(r)$ is the internal inductance. Equation (7) generalizes the formula for circular flux surfaces of Shafranov and Yurchenko [15] and Glasser, Greene and Johnson [16] and is consistent with previous expressions retaining shaping effects near the magnetic axis [14]. Figure 17 shows that (7) is in reasonable agreement with the full Mercier criterion for two equilibria with (a) large aspect ratio A = 10, κ = 1.3 and (b) small aspect ratio A = 2.7, κ = 1.7. Figure 17 also shows the standard Shafranov-Yurchenko expression, which ignores the effect of ellipticity and excludes interchange instability at q = 1.

An approximation of (7) that is sometimes useful for the internal kink mode is obtained by considering almost flat current profiles with q' small and E/r and T/r^2 constant. Together with q = 1, this gives

$$-D_I \approx \frac{1}{4} + \frac{rp'}{s^2B^2}\frac{3E}{r}\left(1 - \frac{8T}{r}\frac{R_0}{r}\right) \tag{8}$$

Equation (8) shows that for sufficient ellipticity, ideal interchange instability can occur for modest pressure and not-so-low shear. As an example, we assume that the pressure profile is parabolic [$\beta_p = -(p'/rB^2)\,(R_0^2q^2/2)$] and that triangularity is negligible. The Mercier criterion then reduces to $\beta_p < s^2/(24e\varepsilon^2)$. Even though the expansion to first order in ellipticity is not very accurate for JET geometry, we consider a JET-like case

with $\varepsilon_{q=1} = 0.16$ and $e_{q=1} = 0.2$ for which (8) gives $\beta_p < 8\ s^2$. This criterion is violated for rather modest pressures when the shear is less than about 0.1. For low shear, say $s \leq 0.03$, even a minute pressure gradient will violate the Mercier criterion at $q = 1$ in an elongated tokamak.

4. SUMMARY

In circular equilibria, the ideal MHD stability of the internal kink is relatively uncomplicated. Our numerical results from full-MHD calculations are in good agreement with the large aspect ratio theory when boundary conditions are properly taken into account. We have modified the large aspect ratio calculation of Bussac et al [1] with respect to the boundary conditions so that it applies for tokamak equilibria with $q_a > 2$. With this modification, most current profiles give β_p-limits that decrease monotonically with increasing $q = 1$ radius. Typically, the large aspect ratio expansion predicts β_p-limits in the range of 0.1 to 0.2, in good agreement our full-MHD results. Both large aspect ratio theory and numerical computations predict instability at low values of q_0 (in combination with high shear at $q = 1$). The stability of the internal kink is dependent on the current profile, e.g., the Shafranov profile is less stable than profiles that are rounded in the central region, while current profiles with shoulders just outside the $q = 1$ surface are more stable.

With regard to shaping, the numerical results show that ellipticity can significantly reduce the β_p-limit. For JET geometry, typical values of the marginal β_p are between 0.05 and 0.1. The reduction of the pressure limit by elongation is accentuated in cases of weak shear in the $q \leq 1$ region. This can be correlated with violation of the Mercier criterion (7).

Finally, we remark that the internal kink mode is a weak MHD instability and can therefore be strongly modified by a multitude of other effects such as resistivity, trapped particles, diamagnetic rotation and electron inertia. Such corrections can be expected to be particularly important when the shear at $q = 1$ is weak and the stability is sensitive to various small effects. In addition, the nonlinear evolution may be different from the indications of linear theory. Nevertheless, it is important to know the result of linear, ideal MHD results with some precision to be able to develop more sophisticated models with confidence.

Acknowledgement: This work was funded in part by the Swiss National Science Foundation.

APPENDIX EXPANSION FOR THE MERCIER CRITERION

The Mercier criterion in axisymmetric geometry is given by [8, 13, 14]

$$- D_I \equiv \left(\frac{p' G I_2}{q'} - \frac{1}{2}\right)^2 + \frac{p'}{q'^2} (I_5' - p' I_3) (G^2 I_1 + I_4) > 0 \quad . \qquad \text{(A1)}$$

Here, the equilibrium field is represented as $\mathbf{B} = \nabla\phi \times \nabla\psi + G(\psi)\,\nabla\phi$, the flux surface integrals are defined as

$$\{I_1, I_2, I_3, I_4, I_5\}$$

$$= \int_{\psi = \text{const}} \frac{J\, d\omega}{2\pi} \left\{ \frac{1}{R^2 |\nabla\psi|^2}, \frac{1}{|\nabla\psi|^2}, \frac{R^2}{|\nabla\psi|^2}, \frac{1}{R^2}, 1 \right\} , \qquad \text{(A2)}$$

and J is the Jacobian from (ψ, ω, ϕ) to Cartesian coordinates.

We now introduce the (r, ω) coordinates as in Eq. (6) and the usual low-beta ordering with β_p finite as $\varepsilon \to 0$. Thus, we write $G = R_0 B_0 g(r)$ with $g = 1 + O(\varepsilon^2)$, $p/B_0^2 = O(\varepsilon^2)$, and $d\psi/dr = R_0 B_0\, \varepsilon f(r)$. The first step of the calculation is to express the components of the metric tensor $g_{rr} = |\partial r/\partial r|^2$, $g_{r\omega} = (\partial r/\partial r) \cdot (\partial r/\partial \omega)$, $g_{\omega\omega} = |\partial r/\partial \omega|^2$ and the Jacobian $J = R\, \partial(R, Z)/\partial(r, \omega)$ as functions of r and ω by differentiating (6). Next, we need equilibrium relations from the Grad-Shafranov equation, which, in (r,ω) coordinates reads

$$\frac{f}{J} \left[\frac{\partial}{\partial r} \left(\frac{f g_{\omega\omega}}{J}\right) - \frac{\partial}{\partial \omega} \left(\frac{f g_{r\omega}}{J}\right) \right] + \frac{p'}{R_0^2 B_0^2} + \frac{g g'}{R^2} = 0 \ , \qquad \text{(A3)}$$

with $' = \varepsilon^{-1}\, d/dr$. The Grad-Shafranov equation is then expanded in ε and e. The ω-independent piece gives the cylindrical pressure balance equation

$$g' + p'/B_0^2 + (f/r)\,(rf)' = 0 \ , \qquad \text{(A4)}$$

that allows to eliminate g'. Equations for the Shafranov shift and the elliptic and triangular deformation of the flux surfaces are obtained from the cos ω component at $O(\varepsilon)$, cos 2ω component at O(e) and cos 3ω component at $O(\varepsilon)$, respectively:

$$\Delta'' + \left(\frac{2f'}{f} + \frac{1}{r}\right)\Delta' = \frac{1}{R_0} - \frac{2rp'}{R_0 B_0^2 f^2}$$

$$+ e\left[E\left(\frac{3p'}{R_0 B_0^2 f^2} - \frac{3\Delta'}{r^2} + \frac{12T}{r^3} + \frac{5T'}{r^2} + \frac{2Tf'}{r^2 f}\right)\right. \qquad \text{(A5)}$$

$$\left. + E'\left(\frac{3rp'}{R_0 B_0^2 f^2} + \frac{3\Delta' f'}{f} + \frac{10T}{r^2} + \frac{2T'}{r} - \frac{3T'f'}{f} - \frac{1}{R_0}\right)\right]$$

$$E'' + \left(\frac{2f'}{f} + \frac{1}{r}\right)E' - \frac{3}{r^2}E = 0 \quad , \qquad \text{(A6)}$$

$$T'' + \left(\frac{2f'}{f} + \frac{1}{r}\right)T' - \frac{8}{r^2}T$$

$$= e\left[E\left(\frac{p'}{R_0 B_0^2 f^2} + \frac{3\Delta'}{r^2}\right) - E'\left(\frac{3rp'}{R_0 B_0^2 f^2} + \frac{4\Delta'}{r} + \frac{3\Delta' f'}{f} - \frac{1}{R_0}\right)\right] . \qquad \text{(A7)}$$

Of course, Eqs (A4 - A7) contain higher order corrections, which do not contribute to the Mercier criterion at the order considered here. For the geometric coefficients, it is convenient to choose the ε^3 terms in (6) [represented by P, although in fact, there are more terms at this order] such that $\int (J/R^2)\, d\omega = 2\pi r/R_0$. (This amounts to defining a free normalization constant at higher order in ε.) With this choice, f can be expressed in terms of the safety factor: $f = rg/qR_0$. To perform the flux surface integrals, we also need $|\nabla r|^2 = g^{rr} = R^2 g_{\omega\omega}/J^2$. To the required order, we obtain

$$I_1 = \frac{R_0^2 q^3}{r^2 G^3}\left[1 + c_0 - 3c_2 - \varepsilon^2\left(\frac{r^2}{R_0^2} + \frac{2\Delta}{R_0}\right) + e\varepsilon^2 E\frac{3r}{2R_0^2}\right] \qquad \text{(A8a)}$$

$$I_2 = \frac{R_0^4 q^3}{r^2 G^3}\left[1 + c_0 + 3c_1 + 3c_2 - \varepsilon^2\left(\frac{3r^2}{2R_0^2} + \frac{4\Delta + 3r\Delta'}{R_0}\right)\right.$$

$$\left. + e\varepsilon^2\frac{9rE + 3r^2E'}{4R_0^2}\right] \qquad \text{(A8b)}$$

$$I_3 = \frac{R_0^6 q^3}{r^2 G^3}\left[1 + c_0 + 6c_1 + 9c_2 - \varepsilon^2 \frac{6\Delta + 6r\Delta'}{R_0} - e\varepsilon^2 \frac{3r^2 E'}{2R_0^2}\right] \tag{A8c}$$

$$I_4 = \frac{q}{G} \tag{A8d}$$

$$I_5 = \frac{R_0^2 q}{G}\left[1 + c_1 - \varepsilon^2\left(\frac{r^2}{2R_0^2} + \frac{2\Delta}{R_0} + \frac{r\Delta'}{R_0}\right) + e\varepsilon^2 \frac{3rE + r^2 E'}{4R_0^2}\right] \tag{A8e}$$

where c_0 contains the $O(\varepsilon^3)$ shaping corrections in (6) and

$$c_1 = e\varepsilon^2 \frac{(rET)'}{rR_0} \quad , \tag{A9a}$$

$$c_2 = e\varepsilon^2 E' \frac{r(\Delta' - T')}{2R_0} \quad . \tag{A9b}$$

Substituting Eqs (A8) into (A1) we obtain expression (7) for the Mercier criterion.

REFERENCES

[1] BUSSAC, M.N., PELLAT, R., EDERY, D., SOULÉ, J.L., Phys. Rev. Lett. **35** (1975) 1638.

[2] de BLANK, H.J., SCHEP, T.J., Phys. Fluids **B3** (1991) 1136.

[3] BONDESON, A., BUSSAC, M.-N., Nucl. Fusion **32** (1992) 513.

[4] TURNBULL, A.D., TROYON, F., Nucl. Fusion **29** (1989) 1887.

[5] CONNOR, J.W., HASTIE, R.J., "The effect of shaped plasma cross sections on the ideal internal kink mode in a tokamak", CLM-M-106 (1985), Culham Laboratory, Abingdon, UK.

[6] BERGER, D., BERNARD, L.C., GRUBER, R., TROYON, F., in *Plasma Physics and Controlled Nuclear Fusion Research 1976*, Proceedings of the 6th International Conference, Berchtesgaden (IAEA, Vienna, 1977), Vol. 2, p. 411.

[7] COPPI, A.C., COPPI, B., Nucl. Fusion **32** (1992) 205.

[8] BONDESON, A., VLAD, G., LÜTJENS, H., "Resistive toroidal stability of internal kink modes in circular and shaped tokamaks" LRP 445/91 (CRPP, Lausanne, 1991), to be published in Phys. Fluids.

[9] LÜTJENS, H., BONDESON, A., ROY, A., Comput. Phys. Comm. **69** (1992) 287.

[10] SOLTWISH, H., STODIEK, W., MANICKAM. J., SCHLÜTER, J., in *Plasma Physics and Controlled Nuclear Fusion Research 1986*, Proceedings of the 11th International Conference, Kyoto (IAEA, Vienna, 1987), Vol. 1, p. 263.

[11] HOLMES, J.A., CARRERAS, B.A., CHARLTON, L.A., Phys. Fluids **B1** (1989) 788.

[12] EDERY, D., LAVAL, G., PELLAT, R., SOULÉ, J.L., Phys. Fluids **19** (1976) 260.

[13] GLASSER, A.H., GREENE, J.M., JOHNSON, J.L., Phys. Fluids **18** (1975) 875; KUVSHINOV, B.N., Sov. J. Plasma Phys. **17** (1991) 79 [Fiz. Plasmy **17** (1991) 139].

[14] FREIDBERG, J.P., in *Ideal Magnetohydrodynamics*, Chap. 10 (Plenum Press, New York, 1987);
LAVAL, G., LUC, H., MASCHKE, E.K., MERCIER, C., PELLAT, R., in *Plasma Physics and Controlled Nuclear Fusion Research 1970*, Proceedings of the 4th International Conference, Madison (IAEA, Vienna, 1971), Vol. 2, p. 507;
LORTZ, D., NÜHRENBERG, J., Nucl. Fusion **13** (1973) 821.

[15] SHAFRANOV, V.D., YURCHENKO, E.I., Sov. Phys. JETP **26** (1968) 682.

[16] GLASSER, A.H., GREENE, J.M., JOHNSON, J.L., Phys. Fluids **19** (1976) 567.

FIGURE CAPTIONS

FIGURE 1 Marginal β_p for circular equilibria from large aspect ratio theory. Results are given for three current profiles: Shafranov (with the step at $r_0 = a/2$) parabolic ($\ell = 1$) and parabolic-squared ($\ell = 2$), in (a) vs. $r_{q=1}/a$ and in (b) vs. q_0.

FIGURE 2 Pressure vs. normalized minor radius ρ for the numerical equilibria.

FIGURE 3 Profiles of (a) averaged toroidal current density I*, (b) safety factor q and (c) shear s vs. ρ for the rounded current profile.

FIGURE 4 Stability limits in β_p for circular equilibrium with aspect ratio 4 and the rounded current profile shown in Fig. 3. (a) β_p vs. $\rho_{q=1}$ and (b) β_p vs. q_0.

FIGURE 5 Internal kink growth-rates vs. β_p for a circular equilibrium with fixed boundary (filled symbols) and free boundary (open symbols). Three different aspect ratios are shown $A = R_0/a = 10$, 5 and 2.7 and $\rho_{q=1} = 0.6$.

FIGURE 6 Profiles of (a) averaged toroidal current density I*, (b) safety factor q and (c) shear s vs. ρ for the flattened current profile with low central shear.

FIGURE 7 Stability limits in β_p for the flattened current profile with low central shear (Fig. 6). The cross section is circular with $A = 4$.

FIGURE 8 Stability limits in β_p for the flattened current profile with higher central shear (four times larger than in Fig. 6). The cross section is circular with $A = 4$.

FIGURE 9 Profiles of (a) averaged toroidal current density I*, (b) safety factor q and (c) shear s vs. ρ for the TEXTOR profile.

FIGURE 10 Stability limits in β_p for the TEXTOR current profile in Fig. 9. The cross section is circular with $A = 4$.

FIGURE 11 Internal kink instability at zero pressure for low q_0, circular equilibrium (A = 4) with the rounded current profile (circles) and the Shafranov profile (squares).

FIGURE 12 Stability limits in β_p for JET geometry and the rounded current profile (Fig. 3).

FIGURE 13 Stability limits in β_p for JET geometry and the flattened current profile with low central shear (Fig. 6). The dashed region indicates violation of the Mercier criterion at q = 1.

FIGURE 14 Stability limits in β_p for JET geometry and the flattened current profile with higher central shear.

FIGURE 15 Stability limits in β_p for JET geometry and the TEXTOR current profile (Fig. 9). The dashed region indicates violation of the Mercier criterion at q = 1.

FIGURE 16 Stability limits in β_p for equilibria with JET geometry and the TEXTOR current profile with reduced shoulders.

FIGURE 17 The Mercier criterion for an equilibrium with elliptic cross section and low shear around the q = 1 surface. The solid line gives the full criterion (A1), the curve with long dashes the large aspect ratio expansion with ellipticity (7), and the curve with short dashes gives the Shafranov-Yurchenko approximation.
(a) aspect ratio A = 10, elongation κ = 1.3 and (b) A = 2.7 and κ = 1.7.

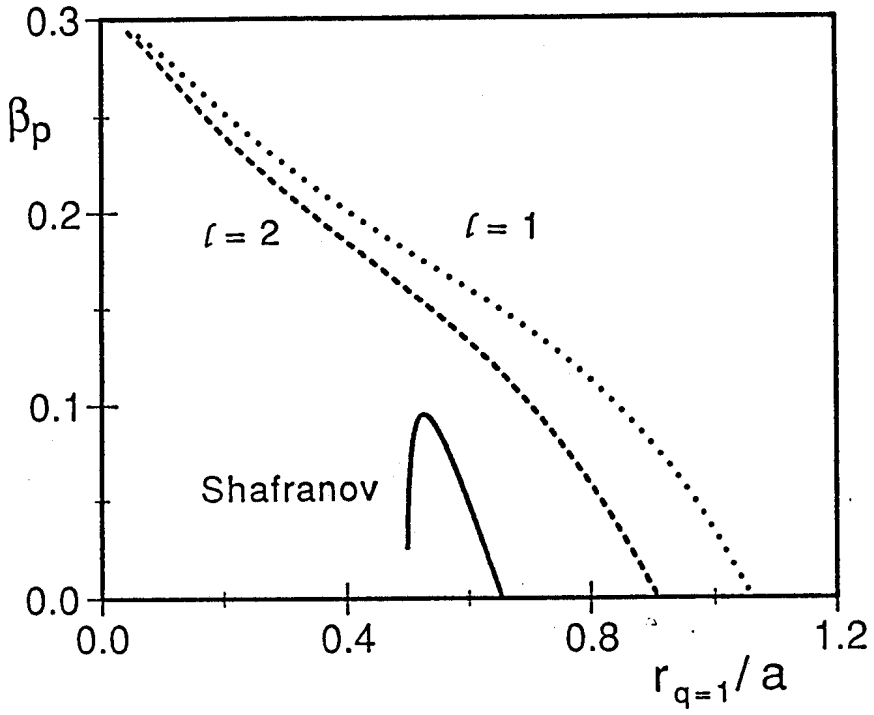

Figure 1a

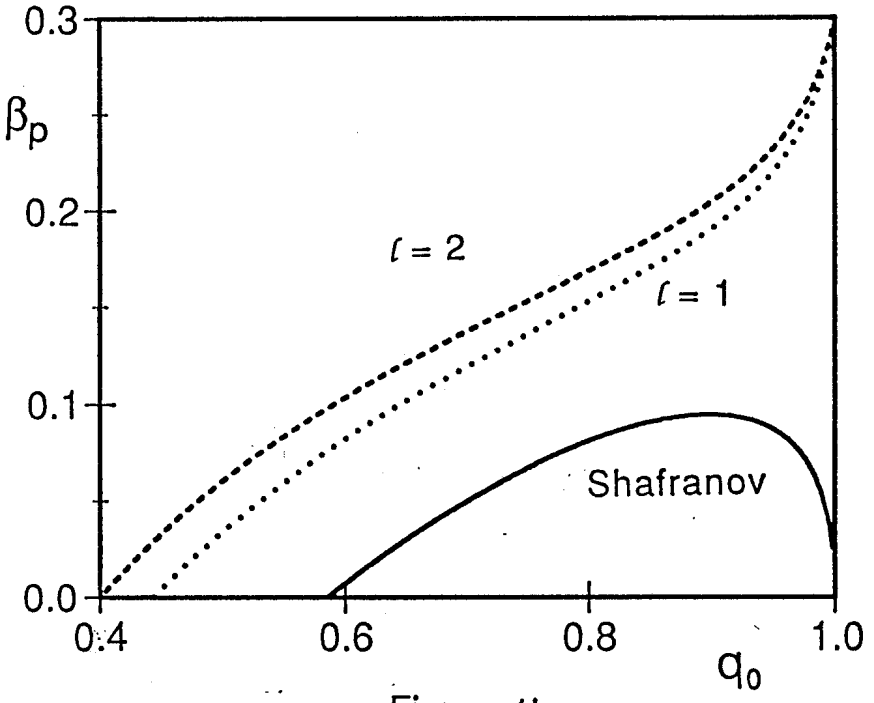

Figure 1b

Figure 2

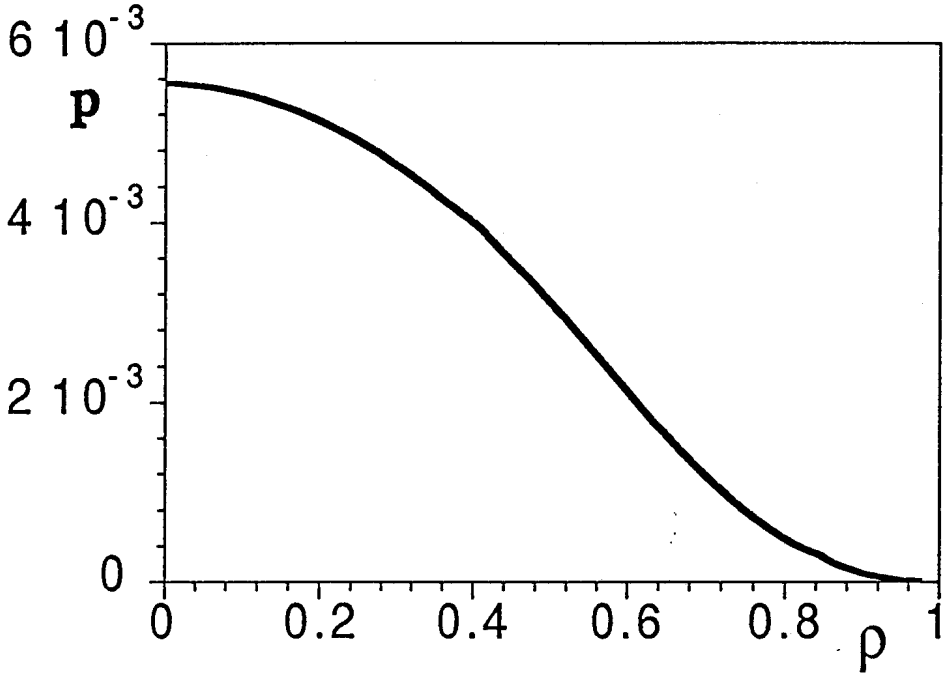

Figure 3a

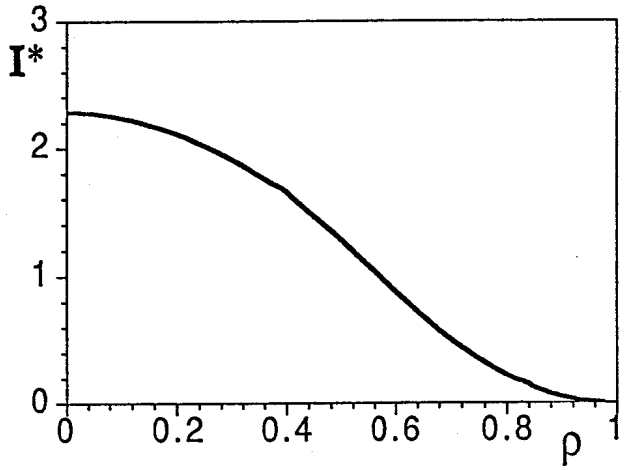

Figure 3b

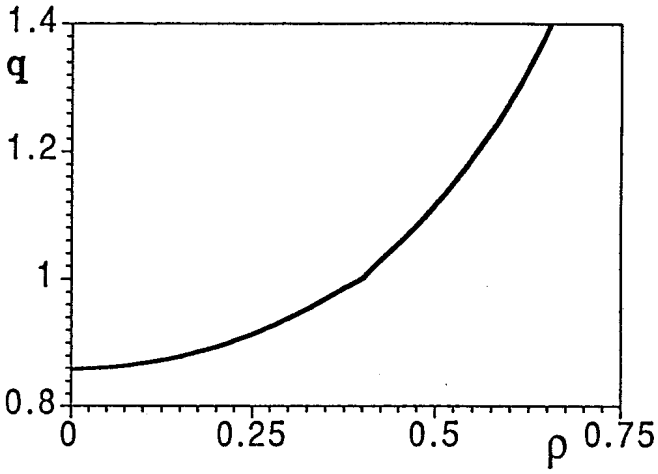

Figure 3c

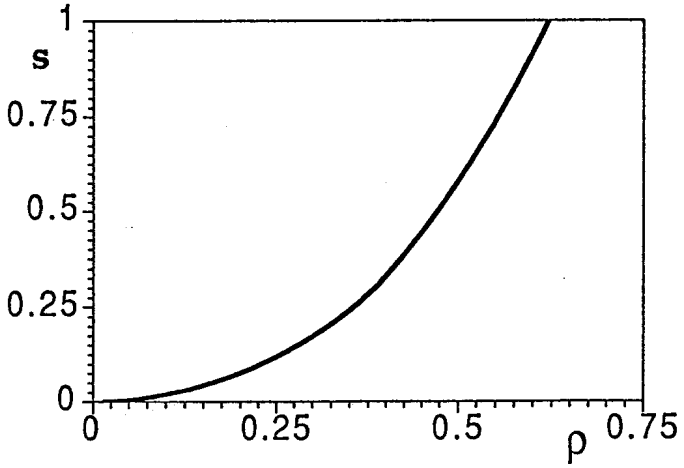

Figure 4a

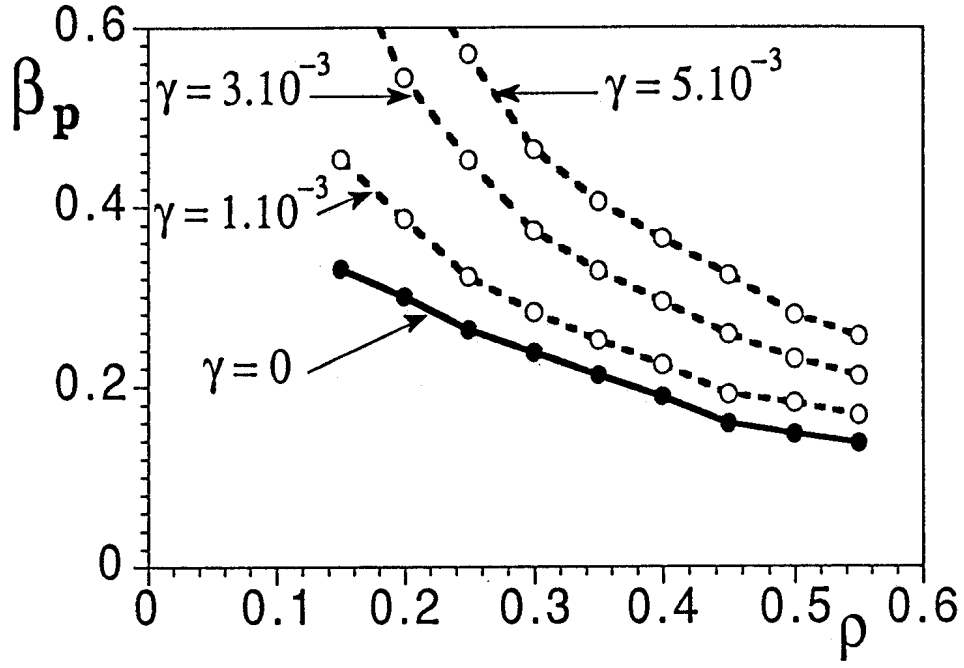

Figure 4b

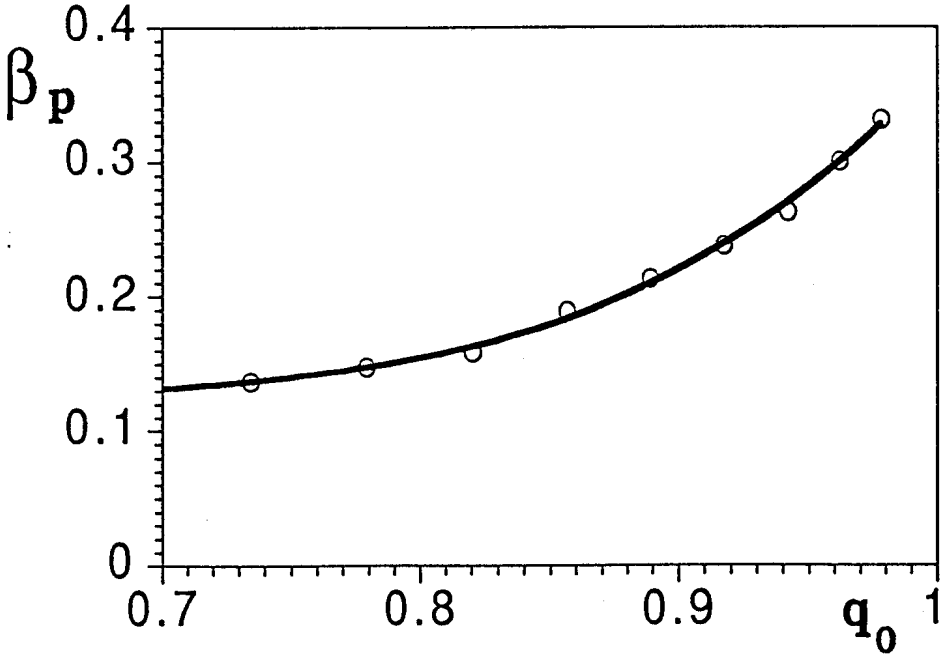

Figure 5

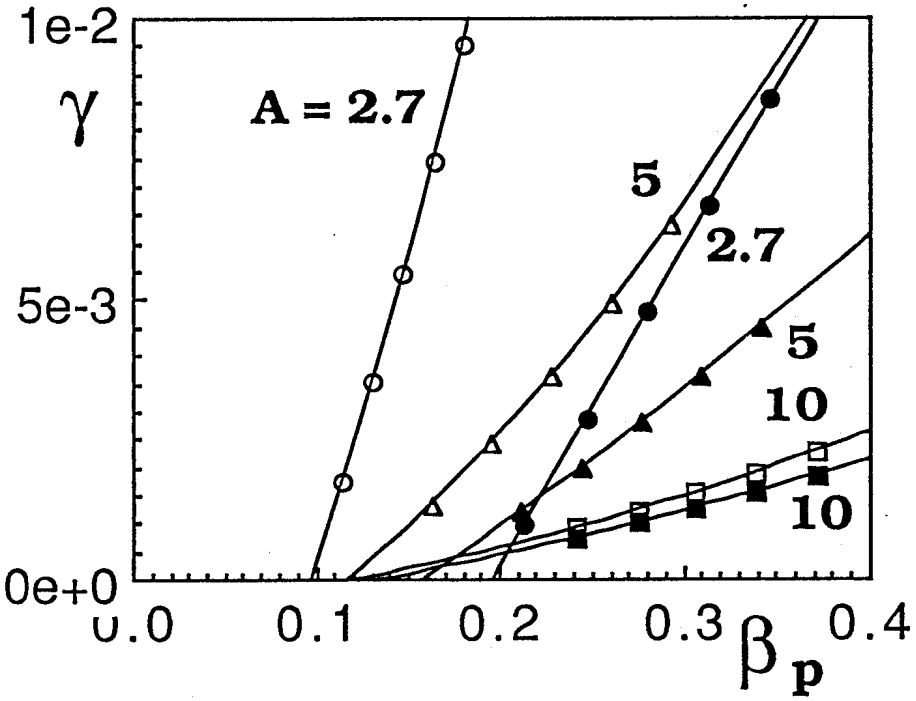

Figure 6a

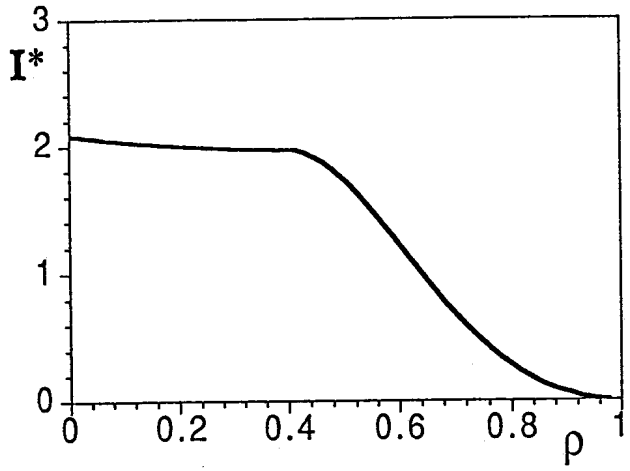

Figure 6b

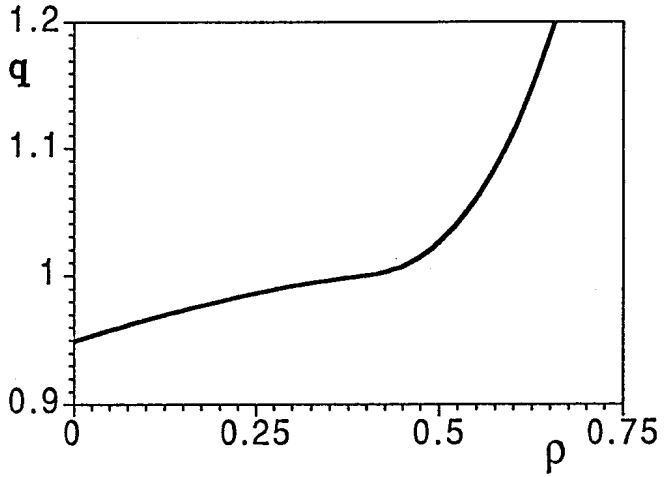

Figure 6c

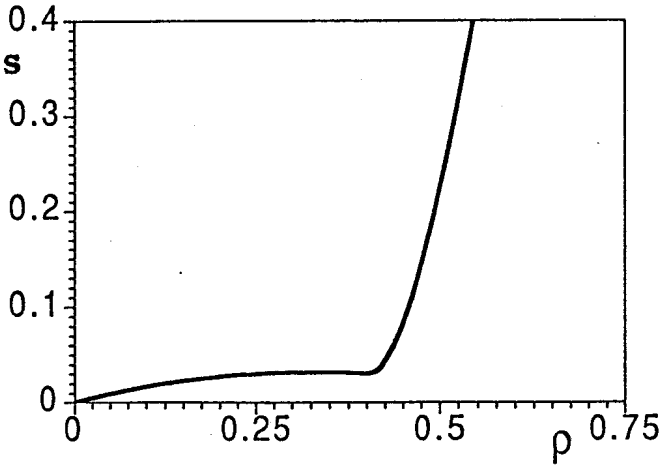

Figure 7

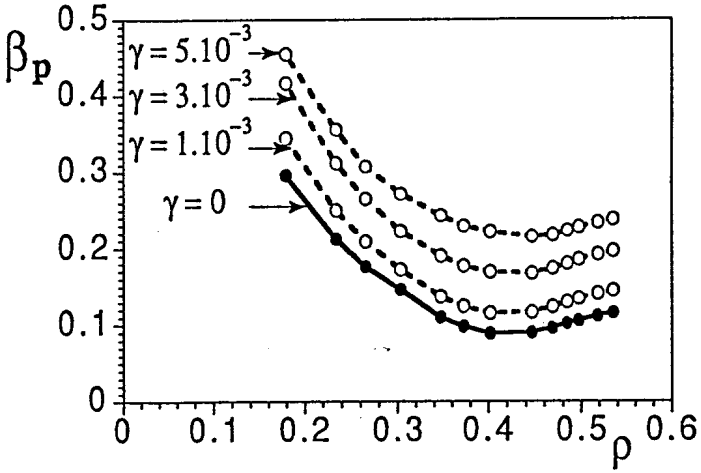

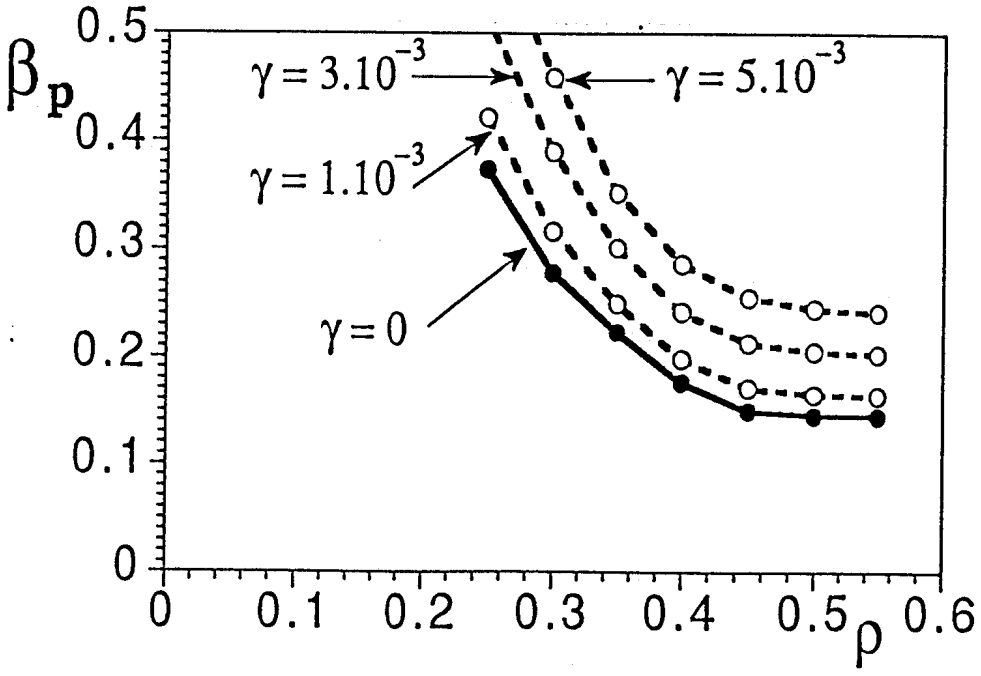
β_p
0.5
0.4
0.3
0.2
0.1
0
$\gamma = 3.10^{-3}$
$\gamma = 5.10^{-3}$
$\gamma = 1.10^{-3}$
$\gamma = 0$
0
0.1
0.2
0.3
0.4
0.5
ρ
0.6

Figure 8

Figure 9a

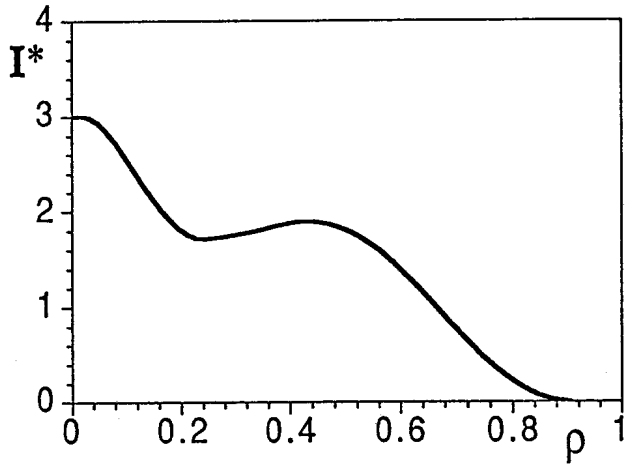

Figure 9b

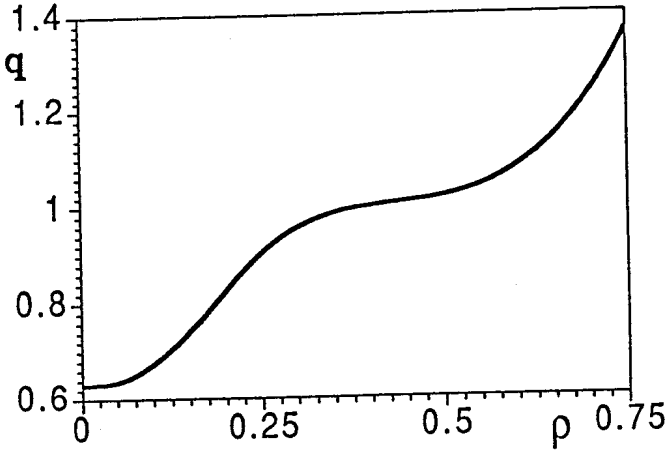

Figure 9c

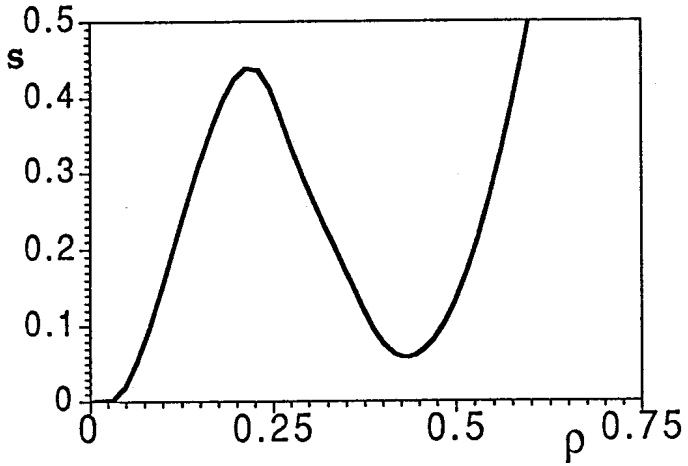

Figure 10

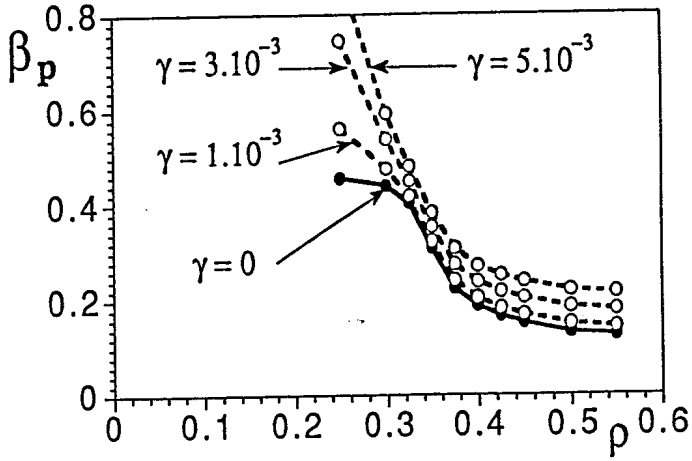

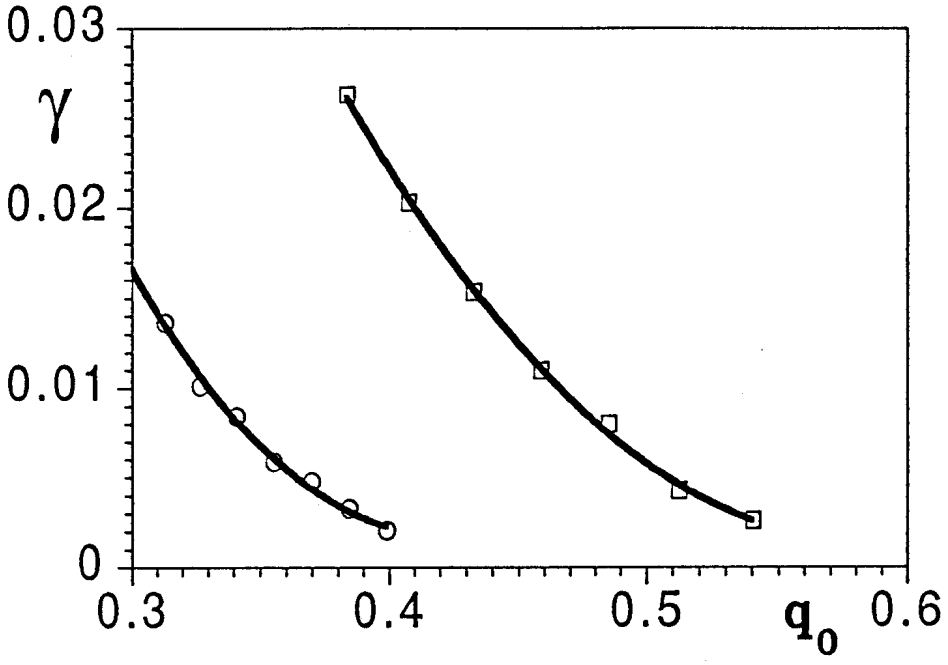

Figure 11

Figure 12

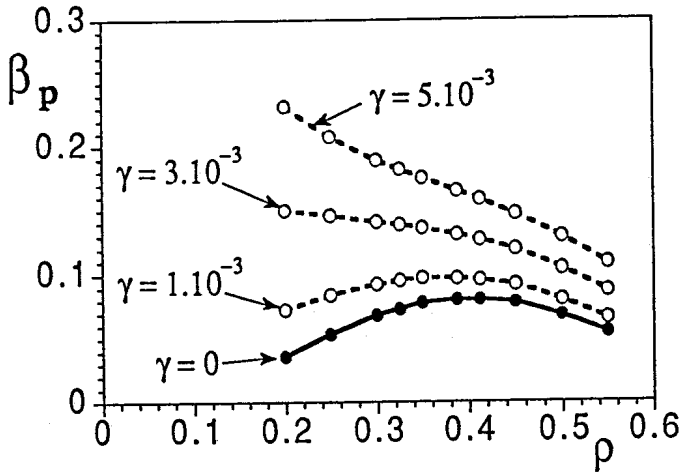

Figure 13

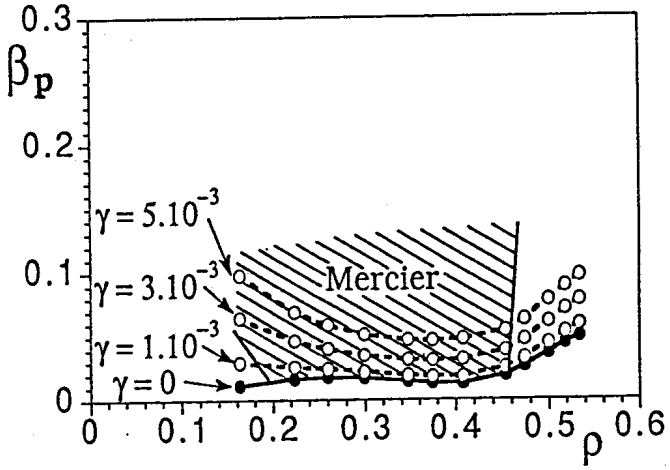

Figure 14

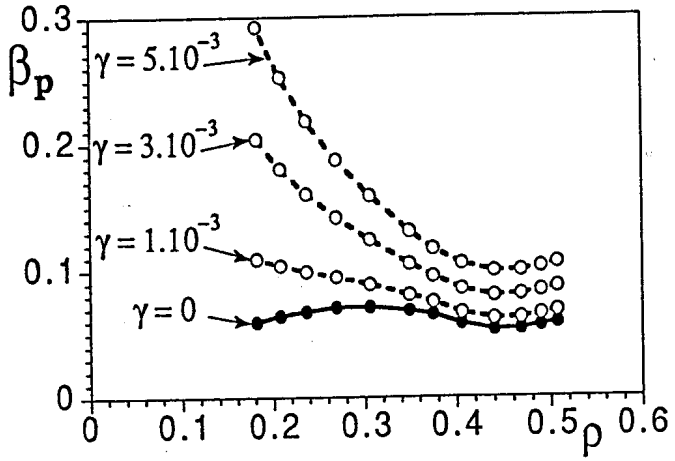

Figure 15

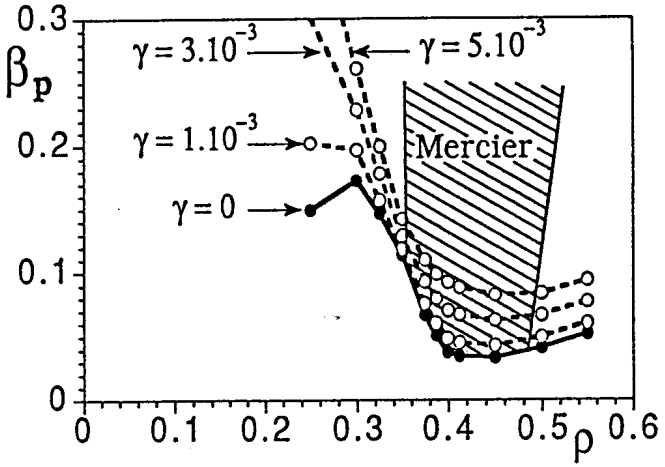

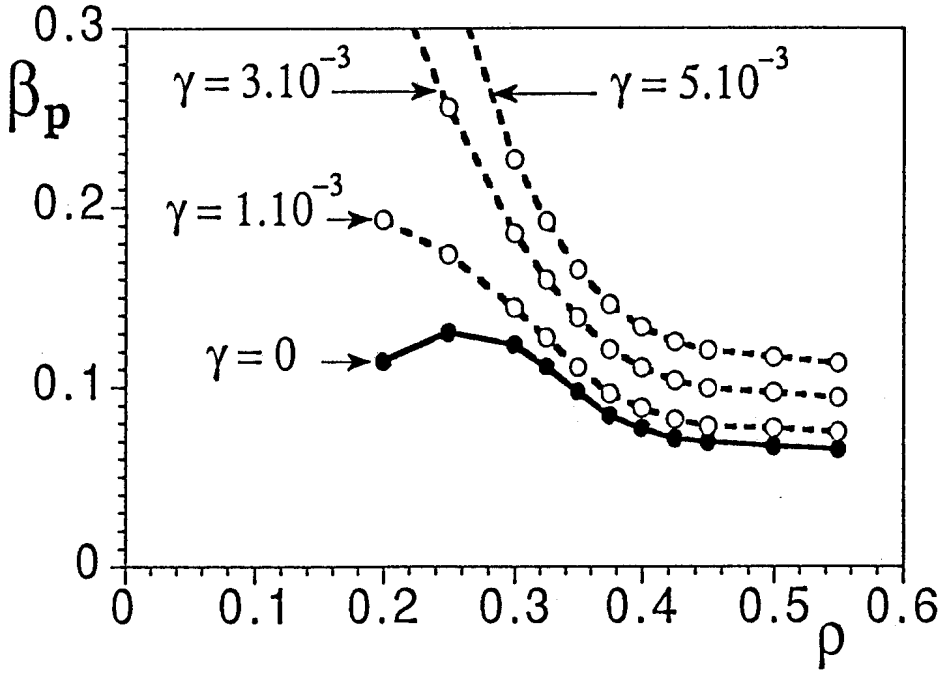
0.3
β_p
0.2
0.1
0
$\gamma = 3.10^{-3}$
$\gamma = 5.10^{-3}$
$\gamma = 1.10^{-3}$
$\gamma = 0$
0
0.1
0.2
0.3
0.4
0.5
0.6
ρ

Figure 16

Figure 17a

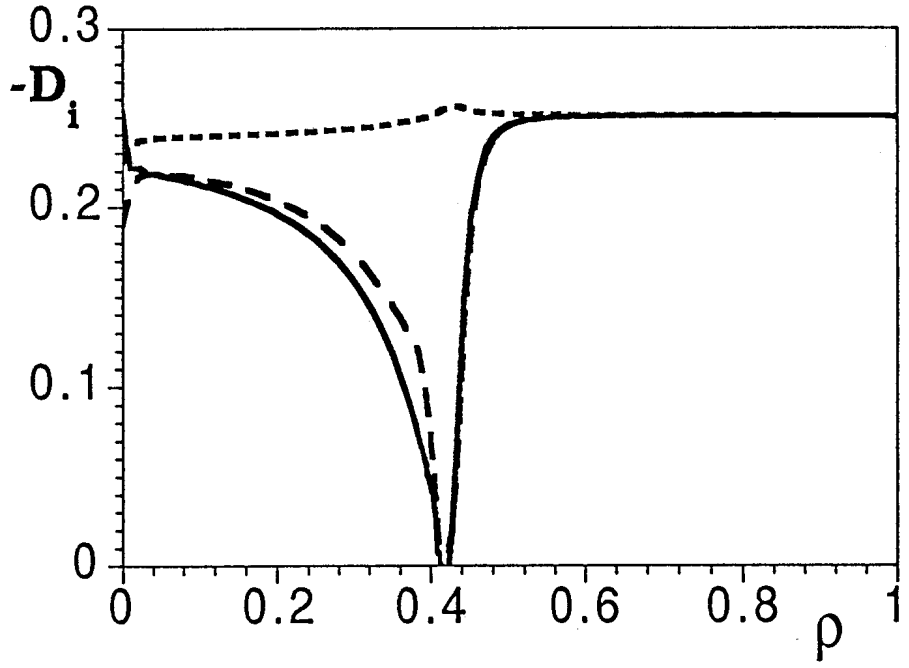

Figure 17b